ISSN 0023-1584, Kinetics and Catalysis, 2008, Vol. 49, No. 5, pp. 682–691. © Pleiades Publishing, Ltd., 2008.
Original Russian Text © A.A. Firsova, T.I. Khomenko, A.N. Il'ichev, V.N. Korchak, 2008, published in Kinetika i Kataliz, 2008, Vol. 49, No. 5, pp. 713–723.

CO Oxidation with Oxygen in the Presence of Hydrogen on CoO/CeO_2 and $CuO/CoO/CeO_2$ Catalysts

A. A. Firsova, T. I. Khomenko, A. N. Il'ichev, and V. N. Korchak

Semenov Institute of Chemical Physics, Russian Academy of Sciences, Moscow, 119991 Russia

e-mail: korchak@center.chph.ras.ru

Received July 13, 2007

Abstract—The catalytic activity of the CoO/CeO_2 and $CuO/CoO/CeO_2$ systems in selective CO oxidation in the presence of hydrogen at 20–450°C ([CuO] = 1.0–2.5%, [CoO] = 1.0–7.0%) is reported. The maximum CO conversion (X) decreases in the following order: $CuO/CoO/CeO_2$ (X = 98–99%, T = 140–170°C) > CoO/CeO_2 (X = 67–84%, T = 230–240°C) > CeO_2 (X = 34%, T = 350°C). TPD, TPR, and EPR experiments have demonstrated that the high activity of $CuO/CoO/CeO_2$ is due to the strong interaction of the supported copper and cobalt oxides with cerium dioxide, which yields Cu–Co–Ce–O clusters on the surface. The carbonyl group in the complexes $Co^{\delta+}$–CO and Cu^+–CO is oxidized by oxygen of the Cu–Co–Ce–O clusters at 140–160°C and by oxygen of the Co–Ce–O clusters at 240°C. The decrease in the activity of the catalysts at high temperatures is due to the fact that hydrogen reduces the clusters on which CO oxidation takes place, yielding Co^0 and Cu^0 particles, which are inactive in CO oxidation. The hydrogenation of CO into methane at high temperatures is due to the appearance of Co^0 particles in the catalysts.

DOI: 10.1134/S0023158408050133

At present, great attention is focused on the development of hydrogen fuel cells as environmentally friendly power sources providing an alternative to internal-combustion engines, which are polluting the atmosphere with greenhouse gases, hydrocarbons, and nitrogen oxides. However, these fuel cells impose stringent requirements on the purity of hydrogen. Because commercial hydrogen is produced from organics, it contains CO, which is poisonous for the platinum electrodes of the fuel cells. Efficient operation of the fuel cells using platinum electrodes is possible only when the carbon monoxide concentration in hydrogen is below 10 ppm; for bimetallic catalysts, such as PtRu, the CO level should be below 100 ppm [1–3]. This degree of purity is expected to be achievable by catalytic, low-temperature, selective CO oxidation with oxygen in the hydrogen medium. This reaction has been extensively investigated on supported systems in which the active component is a noble metal, namely, Pt, Ru, Pd, or Au [1, 4–7], or an oxide such as CoO [8–11] or CuO [12–17]. CuO/CeO_2 catalysts are the most active and the most selective among the Co- and Cu-containing systems. Their high activity is due to the synergetic effect. This effect arises from the strong interaction between the oxides, which yields, on the catalyst surface, highly reactive oxygen capable of oxidizing CO at 100–160°C, much below the CO oxidation temperatures for the pure CuO and CeO_2 oxides ($T \geq 300$°C).

In an earlier study of CO oxidation in excess hydrogen over (0.25–6.4)% CuO/CeO_2 catalysts [17], it was discovered that, as the CuO content is raised, the CO conversion increases and the temperature range of the reaction shifts to lower temperatures by 100°C. The highest CO conversion, 98.5–99.5%, is achieved on (5–6.4%) CuO/CeO_2 at 140–150°C. At $T > 150$°C, the CO conversion decreases because of the dissociative adsorption of hydrogen on active sites and their blocking by adsorbed water. It was also found that CO is adsorbed only on the oxidized catalyst, specifically, $CuO–CeO_2$ clusters, to form CO–Cu^+ carbonyls and is then oxidized by oxygen of these clusters. In order to extend the working temperature range of the Cu/CeO_2 catalysts and to reduce the temperature of maximum CO conversion, we additionally supported iron and nickel oxides, which are inactive in CO oxidation, but can participate in redox processes [18]. The introduction of these oxides into the catalyst increases the number of active sites and CO conversion and extends the oxidation temperature range in the maximum-conversion region.

This work continues the series of our studies in this area and deals with CoO as the admixture. We chose this oxide for the reason that it is active in CO oxidation with oxygen below room temperature [19] and is resistant against poisoning by water vapor at elevated temperatures in CoO_x/CeO_2 systems [9].

The purpose of this study is to determine the activity of the CoO/CeO_2 and $CuO/CoO/CeO_2$ catalysts in CO oxidation with oxygen in excess hydrogen and to gain information about the structure of their active sites and about the reactant adsorption species using temperature-programmed desorption (TPD) and temperature-

programmed reduction (TPR) techniques and EPR spectroscopy.

EXPERIMENTAL

Cerium dioxide (S_{sp} = 70 m^2/g) was obtained by heating $Ce(NO_3)_3 \cdot 6H_2O$ to 500°C at a rate of 7 K/min in air followed by calcination at this temperature for 2 h. The specific surface area of catalysts was measured by the BET method using low-temperature argon adsorption.

CoO/CeO_2 catalysts were prepared by impregnating cerium dioxide with a cobalt nitrate solution followed by drying at 150°C and calcination at 500°C for 2 h. The CoO content of the catalysts was 1, 2.5, 3.5, 5, or 7 wt %. The surface concentration of Co cations varied between 1.1×10^{18} and 8.0×10^{18} ion/m^2.

CuO was supported on the CoO/CeO_2 catalysts by impregnating them with a copper nitrate solution, drying at 150°C, and calcination at 500°C for 2 h. The resulting $CuO/CoO/CeO_2$ catalysts contained 1 or 2.5 wt % CuO.

The synthesized catalysts were characterized by X-ray powder diffraction on a DRON-3M diffractometer calibrated against a SiO_2 (α-quartz) powder. The diffraction patterns of the samples in the $2\theta = 8°–70°$ range showed reflections characteristic of the fcc (*Fm*3*m*) cerium dioxide phase. The particle size of cerium dioxide was ~15 nm as determined using the Debye–Scherrer formula. This value is in good agreement with the particle size of 10–13 nm reported for CeO_2 samples prepared by the decomposition of cerium hydroxide and carbonate at 500°C [20]. We observed no effect of the supported copper and cobalt oxides on the reflection width. The X-ray diffraction patterns showed no reflections assignable to the supported oxides. This can be due to either the low concentration of these oxides or their high degree of amorphism.

CO oxidation with oxygen in excess hydrogen was carried out in a flow apparatus. The feedstock, which consisted of 98 vol % H_2, 1 vol % CO, and 1 vol % O_2, was passed through a tubular quartz reactor 3 mm in diameter filled with a catalyst (20 mg). The products were identified chromatographically using two columns, one packed with molecular sieve NaX (13 Å) and the other with Porapak QS, and thermal-conductivity detectors. The Co-to-CO_2 conversion will be designated *X*, and the maximum-conversion temperature will be designated T_{max}.

CO adsorption species were studied by vacuum TPD. The catalyst sample (100 mg) was preheated in a vacuum ($P = 10^{-4}$ Pa) at 500°C for 1 h, treated with oxygen at $P = 2 \times 10^2$ Pa for 20 min, cooled to room temperature, and pumped. Next, CO ($P_{CO} = 2 \times 10^{-2}$ Pa) was adsorbed onto the surface of the oxidized sample for 5 min. Thereafter, the sample was heated at a rate of 10 K/min under continuous pumping. TPD spectra as the desorption rate (*W*, arb. units) versus temperature (*T*) were obtained using a Pirani gage with an automated recording system [21]. The composition of the desorbed gas was monitored with an MX-7304 mass spectrometer. The desorbed CO and CO_2 were separated by freezing the CO out in a U-shaped liquid-nitrogen trap placed between the reactor and the Pirani gage. This technique allowed us to record both the CO + CO_2 desorption spectrum and the desorption spectrum of CO alone. In addition, the subtraction of the latter from the former yielded the CO_2 desorption spectrum. The amount of desorbed gas was determined by measuring the gas pressure in the closed reactor in another run.

CO, O_2, and H_2 were obtained by standard procedures [22]. In order to remove the impurities that were not controlled (CO_2 and H_2O), the gases to be admitted to the sample surface were passed through a liquid-nitrogen trap.

The *X*-band EPR spectra of samples oxidized at $P_{O_2} = 2 \times 10^2$ Pa and $T = 500°C$ were recorded in a vacuum (10^{-4} Pa) or in a gas medium at –196 or 20°C on an EPR-V spectrometer equipped with a Diapazon temperature attachment. The number of paramagnetic species was determined by doubly integrating the EPR spectra and comparing the result with the same data for $CuSO_4 \cdot 5H_2O$ as the reference. The accuracy of EPR measurements was 20%.

The TPR of catalysts was carried out in a 6% H_2 + Ar mixture flowing at a rate of 100 ml/min. The products were identified using a thermal-conductivity detector. The sample was heated from 20 to 650°C at a rate of 12 K/min. Before a TPR run, the sample (100 mg) was calcined in flowing air at 500°C for 1 h. Hydrogen uptakes were derived from TPR peak areas with an accuracy of ~10%.

RESULTS

Catalytic Activities of CeO_2, CoO/CeO_2, and $CuO/CoO/CeO_2$ in CO Oxidation with Oxygen in Excess Hydrogen

Catalytic tests of CeO_2, CoO/CeO_2, and $CuO/CoO/CeO_2$ were performed in the temperature range from 20 to 450°C. At low temperatures of 20–200°C, CeO_2 is inactive, and only at 300–350°C does the conversion *X* reach 25–35% (Fig. 1, curve *1*). The CeO_2 catalysts containing supported cobalt oxide are substantially more active. For the CoO/CeO_2 sample containing 1.0% CoO (Fig. 1, curve *2*), *X* = 67% at T_{max} = 230–240°C. As the CoO content is raised to 2.5, 3.5, 5, and 7 wt %, *X* increases to 72.5, 78.5, 80, and 84%, respectively, at T_{max} = 230–240°C (Fig. 1, curves *3–6*). As the temperature is raised further, *X* falls sharply and methane appears among the reaction products, which results from CO hydrogenation. This reaction sets in at 260–270°C on the (2.5–7)% CoO/CeO_2 catalysts. At 400–450°C, carbon monoxide turns

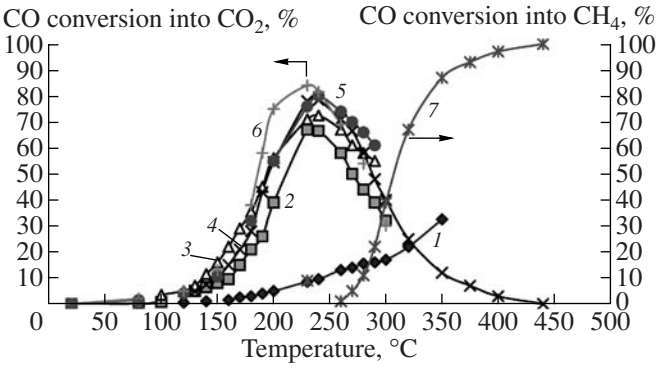

Fig. 1. Temperature dependence of the CO conversion into (*1–6*) CO_2 and (*7*) CH_4 on *n*% CoO/CeO_2 catalysts: *n* = (*1*) 0, (*2*) 1, (*3*) 2.5, (*4, 7*) 3.5, (*5*) 5, and (*6*) 7.

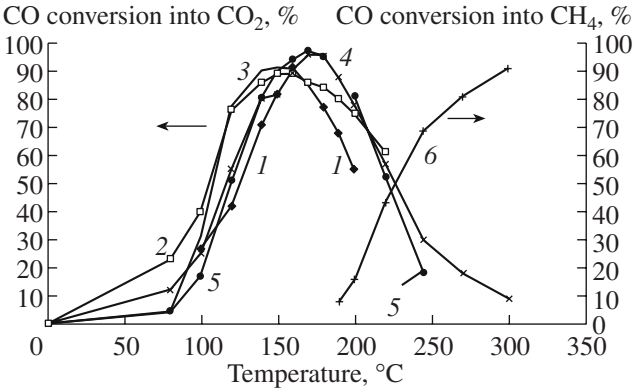

Fig. 2. Temperature dependence of the CO conversion into (*1–5*) CO_2 and (*6*) CH_4 on 1% CuO/*n*% CoO/CeO_2 catalysts: *n* = (*1*) 0, (*2*) 1.0, (*3*) 2.5, (*4, 6*) 3.5, and (*5*) 7.0.

entirely into methane (the conversion of CO into CH_4 is 100%). By way of example, Fig. 1 plots the temperature dependence of the CO-to-CH_4 conversion for the 3.5% CoO/CeO_2 catalyst (curve *7*).

The supporting of 1% CuO on the CoO/CeO_2 surface markedly changed the properties of the catalyst (Fig. 2). The maximum value of *X* was attained at T_{max} = 140–170°C, as distinct from T_{max} = 230–240°C for CoO/CeO_2, and the hydrogenation onset temperature was lower by 80–90°C. No hydrogenation was observed with catalysts containing 1% CuO and 1.0–2.5% CoO.

It follows from the data presented in Fig. 2 that not only does CuO affect the properties of CoO/CeO_2, the properties of CuO/CeO_2 [17] are also altered by CoO. The introduction of cobalt oxide into the 1% CuO/CeO_2 catalyst raises its activity (*X* at T_{max} = 140–170°C increases from 89 to 98%) and extends the temperature range of maximum CO-to-CO_2 conversion both to lower temperatures (by ~20°C) and to higher temperatures (by ~25–30°C).

The activity of the CuO/CeO_2 catalyst increases as the copper oxide content is increased from 1 to 2.5 wt %: *X* rises from 89 to 95% and T_{max} decreases from 160 to 140°C [17]. A similar effect is observed for the $CuO/CoO/CeO_2$ catalysts: raising the CuO content from 1 to 2.5% reduces T_{max} to 145°C and increases *X* to 97.5%.

In order to see how the activity of the catalyst in CO oxidation into CO_2 depends on the order in which copper and cobalt oxides are supported on the cerium dioxide surface, we synthesized the samples 2.5% CuO/2.5% CoO/CeO_2 (*1*) and 2.5% CoO/2.5% CuO/CeO_2 (*2*). In sample 1, CeO_2 was loaded first with CoO and then with CuO; in sample 2, CuO was supported first. The maximum conversion of CO into CO_2 on these samples was nearly the same (97.5%); however, it was reached at 145°C with sample 1 and at 175°C with sample 2. These data suggest that the composition of the active sites on the catalyst surface depends on the order in which the copper and cobalt oxides were supported.

CO Adsorption and Oxidation on CeO_2, CoO/CeO_2, CuO/CeO_2, and $CuO/CoO/CeO_2$ Catalysts According to TPD Data

Desorption from the CeO_2 surface is observed only at $T > 400$°C (Fig. 3, curve *1*). The number of desorbed molecules per unit area of the surface is 2.0×10^{16} m^{-2}. The only TPD product released by the surface of oxidized CeO_2 is CO_2. It likely forms by the decomposition of the surface carbonates that have resulted from CO adsorption, as is suggested by the fact that the TPD spectrum of the oxidized sample on which CO was not adsorbed does not show any desorption peaks. Furthermore, the CO_2 desorption temperature range coincides with the temperature range of the decomposition of the surface carbonates on CeO_2 [20]. As the CO adsorption

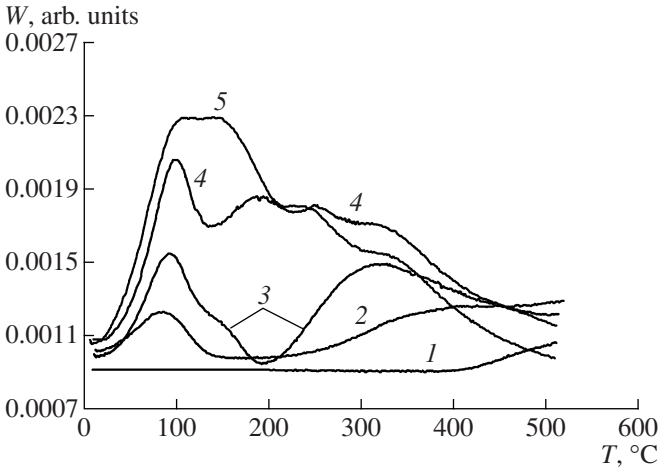

Fig. 3. TPD spectra recorded after CO adsorption at 20°C for 5 min on oxidized (*1*) CeO_2, (*2*) 1% CuO/CeO_2, (*3*) 2.5% CuO/CeO_2, (*4*) 1% CuO/2.5% CoO/CeO_2, and (*5*) 2.5% CuO/2.5% CoO/CeO_2.

temperature is raised from 20 to 250°C, the onset temperature of CO_2 desorption decreases to 350°C and the amount of desorbed CO_2 increases from 2.0×10^{16} to 1.0×10^{17} m^{-2}. This finding indicates that carbonate formation on CeO_2 is an activated process and is in agreement with earlier studies [20, 23].

The TPD spectra of the 1% CuO/CeO_2 and 2.5% Co/CeO_2 samples consist of two peaks (Fig. 3, curves *2*, *3*). The first peak, which occurs at $T_{max,des}$ = 100°C, is due to CO desorption. The second, composite peak, observed in the temperature range from 200 to 500°C, is due to CO_2 desorption. The numbers of CO and CO_2 molecules desorbed from the 2.5% Co/CeO_2 sample are 3.3×10^{17} and 4.4×10^{17} m^{-2}, respectively. For the 1% CuO/CeO_2 sample, these numbers are 1.7×10^{17} and 3.1×10^{17} m^{-2}, respectively. CO desorption arises from the decomposition of the carbonyl complexes Cu^+–CO and $Co^{\delta+}$–CO, which, according to an earlier report [24], result from CO adsorption on oxidized copper and cobalt cations at 20°C and decompose at 100°C. This is in agreement with our data. The fact that the supported catalysts, as compared to cerium dioxide, desorb CO_2 in larger amounts and at lower temperatures down to 200°C is evidence of the formation of new CO adsorption and oxidation sites involving copper oxides (Cu–ox) and cobalt oxides (Co–ox). (Here, ox stands for a CO adsorption and oxidation surface site.)

The TPD profiles of the 1% Co/CeO_2 and 7% Co/CeO_2 samples are identical in shape to that of the 2.5% Co/CeO_2 sample. However, reducing the CoO content to 1% decreases the amount of desorbed CO and CO_2 by a factor of ~2 and raising the CoO content to 7% increases their amount by a smaller factor of 1.2. Changing the amount of copper oxide in CuO/CeO_2 from 1.0 to 2.5% does not alter the character of the TPD spectrum, but it causes an increase in the amounts of desorbed CO and CO_2 [17].

The TPD spectrum of the 1% $CuO/2.5\%$ CoO/CeO_2 catalyst differs significantly from the spectra of the 1% CuO/CeO_2 and 2.5% CoO/CeO_2 samples (Fig. 3, curves *2–4*). The decomposition of the former into the TPD profiles of the desorption products CO and CO_2 is shown in Fig. 4. It is clear that, in the temperature range examined, CO desorption at $T_{max,des}$ = 100°C (curve *2*) takes place along with CO_2 desorption (curve *3*). The amount of desorbed CO is 4.1×10^{17} m^{-2}, and the amount of desorbed CO_2 is 7.2×10^{17} m^{-2}. This amount of CO is equivalent to the total number of CO molecules desorbed owing to the decomposition of the carbonyl complexes on the surfaces of the 1% CuO/CeO_2 and 2.5% CoO/CeO_2 samples. Therefore, the surface of the catalyst contains both Cu^+–CO and $Co^{\delta+}$–CO. The overlap of the CO_2 TPD spectra of 1% CuO/CeO_2, 2.5% CoO/CeO_2, and 1% $CuO/2.5\%$ CoO/CeO_2 between 200 and 500°C (Fig. 3) suggests that the third catalyst contains the same CO oxidation sites as the first two. At the same time, CO_2 desorption at 50–200°C is

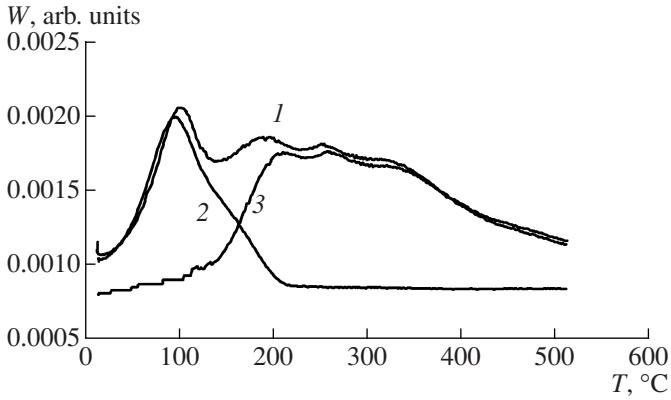

Fig. 4. TPD spectra of the 1% $CuO/2.5\%$ CoO/CeO_2 sample (O_2, 50°C) after CO adsorption on it at 20°C: (*1*) CO + CO_2, (*2*) CO, and (*3*) CO_2.

evidence that the ternary system $CuO/CoO/CeO_2$ has low-temperature CO oxidation sites (Cu–Co–ox), which are absent in the binary systems in the supported oxide content ranges examined. The number of Cu–Co–ox sites depends on the amounts of the supported oxides in the ternary system. As the amount of copper oxide is increased from 1 to 2.5% (Fig. 3, curves *4*, *5*), the concentration of Cu–Co–ox sites increases. At the same time, their concentration decreases as the cobalt oxide content is decreased. This dependence of the number of Cu–Co–ox sites on the CuO and CoO contents of the ternary system suggests that these sites result only from the interaction of all three oxides (CuO, CoO, and CeO_2). In the CoO and CuO content range 1–2.5%, the number of Cu–Co–ox sites is independent of the order in which the oxides were supported. Thus, part of the adsorbed CO molecules in the ternary system $CuO/CoO/CeO_2$ form the carbonyls Cu^+–CO and $Co^{\delta+}$–CO and the others are oxidized by surface oxygen on the Cu–Co–ox sites.

The CO oxidation reaction takes place in the presence of hydrogen. For this reason, we studied the CO and CO_2 adsorption species after treatment of the oxidized 1% $CuO/2.5\%$ CoO/CeO_2 sample with hydrogen at T_{H_2} = 50, 100, 140, or 180°C for 10 min. In this case, after the sample was reduced in hydrogen at a preset temperature, it was pumped and cooled to room temperature. Next, CO was adsorbed and the TPD spectrum was recorded (Fig. 5). Spectrum *1* in Fig. 5 (T_{H_2} = 50°C) coincides with spectrum *4* in Fig. 3, which was obtained after CO adsorption onto the oxidized sample. As T_{H_2} is raised from 100 to 180°C (Fig. 5, curves *2–4*), the intensity of the CO_2 desorption peak at 160°C decreases, and it is close to zero for T_{H_2} = 140 and 180°C (curves *3*, *4*). Spectra *3* and *4* consist of two peaks. One of them (100°C) is due to CO desorption. The other, composite peak occurs at 200–500°C and is due to CO_2 desorption. These spectra are similar to the

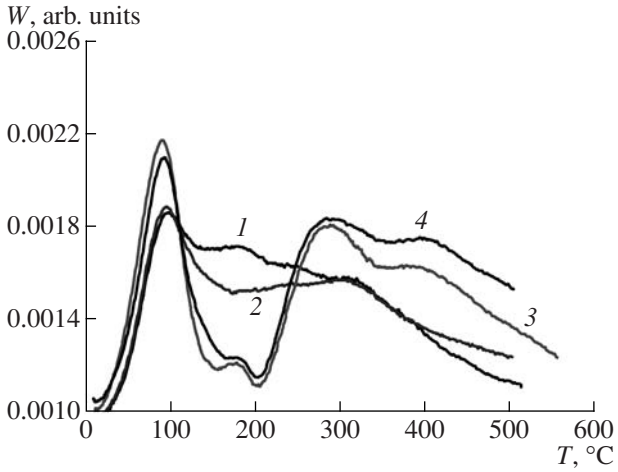

Fig. 5. TPD spectra of the oxidized 1% CuO/2.5% CoO/CeO_2 sample after its reduction in hydrogen for 10 min at T = (*1*) 50, (*2*) 100, (*3*) 140, and (*4*) 180°C followed by pumping at these temperatures and CO adsorption at 20°C for 5 min.

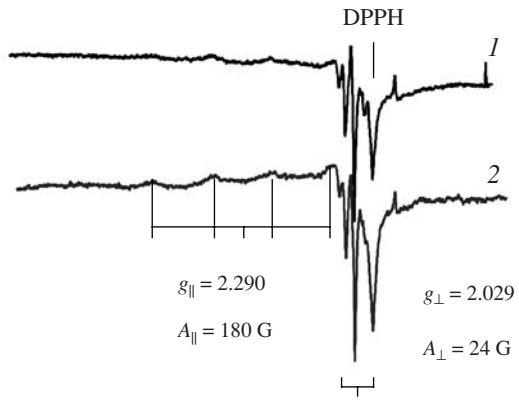

Fig. 6. EPR spectra of 2.5% CoO/2.5% CuO/CeO_2 at –196°C: (*1*) sample in vacuo; (*2*) sample containing CO adsorbed at 20°C.

spectrum recorded after CO adsorption on the surface of the oxidized 2.5% CoO/CeO_2 sample (Fig. 3, curve *3*). This coincidence of the spectra suggests that oxygen of only Cu–Co–ox sites reacts with hydrogen, resulting in the reduction of the copper cations to Cu^0, a copper state inactive in CO adsorption and oxidation [18]. The water that formed at 100–180°C was pumped away and, as a consequence, did not show itself in the TPD spectrum during CO_2 desorption from Co–ox. Therefore, the treatment of the 1% CuO/2.5% CoO/CeO_2 catalyst with hydrogen at T_{H_2} ~ 140°C does not affect the CO oxidation activity of the Co–ox sites, but destroys the Cu–Co–ox sites. After the deeper reduction of the 2.5% CoO/CeO_2 and 1% CuO/2.5% CoO/CeO_2 catalysts in hydrogen at 500°C for 5 min, their TPD spectra show only two CO peaks in the 30–350°C range and are identical. The amount of desorbed CO in this case is 3.7×10^{17} m^{-2}. According to [24], the desorption peaks at 100 and 160°C are due to the decomposition of the $Co^{\delta+}$–CO and Co^0–CO complexes, respectively. The amount of the $Co^{\delta+}$–CO complexes is ~6 times smaller than the amount of the Co^0–CO complexes.

Thus, the surface of the reduced 2.5% CoO/CeO_2 and 1% CuO/2.5% CoO/CeO_2 catalysts is dominated by copper and cobalt metal particles, which are inactive in CO oxidation.

EPR Data for the Cu^{2+} Cation in the CuO/CoO/CeO_2 Catalysts

Figure 6 (curve *1*) shows the EPR spectrum of 2.5% CoO/2.5% CuO/CeO_2 (sample 2) recorded in a vacuum at –196°C. This axisymmetric signal arises from the interaction between the electron spin s = 1/2 and the nuclear spin I = 3/2 [25] and has the following tensor parameters: $A_{\|}$ = 180 G, $g_{\|}$ =2.290, $A_{\perp}$ = 25 G, and $g_{\perp}$ = 2.028. A similar signal was observed for the CoO-free oxidized sample 2.5% CuO/CeO_2 [17]. Since the paramagnetic cation Ce^{3+} in CeO_2 does not show itself in the EPR spectrum because of the short spin–lattice relaxation time [26, 27], there is good reason to believe that the spectrum considered refers to isolated Cu^{2+} cations coordinated to oxygen anions of the CeO_2 surface, thus forming Cu^{2+} oxo complexes.

The coordination polyhedra of copper cations on oxide surfaces vary from a distorted octahedron to a square pyramid and a planar square [28]. In our case, the *g*- and *A*-tensor parameters are similar to the values observed for the square-planar coordination of Cu^{2+} in ZSM-5 zeolites [29]. The adsorption of molecules on these copper cations must modify spectral parameters because of the change in the number of ligands in the coordination spheres of the cations. However, the adsorption of H_2, NH_3, and NO molecules ($P = 2 \times 10^2$ Pa, T = 20°C) on the 2.5% CoO/2.5% CuO/CeO_2 catalyst does not change the EPR spectral intensities and parameters. This indicates that these molecules do not interact with the Cu^{2+} cation in its oxo complexes. The adsorption of CO on the same sample raises the intensity of the EPR signal by a factor of 2 without changing its *g*- or *A*-tensor (Fig. 6, curve *2*). The adsorption of CO on the 2.5% CuO/CeO_2 sample changes neither the intensity nor the parameters of the EPR spectrum. Furthermore, the intensity of the Cu^{2+} signal decreases as the cobalt content of the sample is increased. It follows from these data that the Cu^{2+} ions of the 2.5% CoO/2.5% CuO/CeO_2 sample that are observed in the EPR spectrum are inaccessible to gases and are likely localized in a subsurface layer of CeO_2, while the cobalt ions occur on the very surface.

The strengthening of the Cu^{2+} signal caused by CO adsorption on the 2.5% CoO/2.5% CuO/CeO_2 sample can be explained as follows. The paramagnetic cation Co^{2+} located near a Cu^{2+} ion shortens the spin–lattice

relaxation time (t_1) of the latter. As a consequence, part of the Cu^{2+} ions may be unobservable in the EPR spectrum. However, after CO adsorption, the effect of the Co^{2+} ions is weaker and, accordingly, t_1 is longer, so the Cu^{2+} ion can be detected by EPR.

The concentration of Cu^{2+} oxo complexes in the 2.5% CoO/2.5% CuO/CeO_2 sample is 4.0×10^{16} ion/m^2, which is nearly one order of magnitude lower than their concentration in the 2.5% CuO/CeO_2 sample (3.2×10^{17} ion/m^2). On the other hand, both before and after CO adsorption on 2.5% CoO/2.5% CuO/CeO_2, the amount of Cu^{2+} oxo complexes in this sample does not exceed 3% of the supported copper cations and, according to TPD data, is approximately one order of magnitude smaller than the amount of adsorbed and oxidized CO. Therefore, the Cu^{2+} oxo complexes are not CO oxidation sites.

TPR Data for the CoO/CeO_2 and $CuO/CoO/CeO_2$ Catalysts

We observed two peaks at 400 and 526°C in the TPR spectrum of CeO_2. According to earlier data [30–32], the TPR spectrum of CeO_2 may contain one to three peaks: a peak at ~450°C, which arises from the reduction of the surface; a peak at ~580°C, which is due to the formation of nonstoichiometric oxides of composition CeO_x; and a peak at ~920°C, which indicates the reduction of CeO_2 to Ce_2O_3 in the sample bulk. The peaks observed in our study are likely due to the reduction of the surface and the formation of nonstoichiometric oxides.

At low CoO contents (1%) of CeO_2, the spectrum shows two broad overlapping peaks at 263 and 330°C (Fig. 7, curve *2*) and the high-temperature peaks due to the reduction of the CeO_2 surface (400 and 526°C) are missing. Both the peak positions and the shape of the spectrum are not typical for bulk Co_3O_4 [33] or other systems containing supported cobalt (CoO/SiO_2, CoO/Al_2O_3) [34–36]. For these systems, the cobalt reduction peaks occur at higher temperatures and the intensity of the first peak is usually 1/3 of the intensity of the second. These peaks correspond to the consecutive reduction of Co_3O_4 to CoO and then Co^0. In our case, the peak positions and shapes are evidence that the cobalt and cerium oxides interact profoundly and that cobalt is most likely present as CoO.

Raising the CoO content of the catalyst to 2.5% causes an increase in the intensity of the hydrogen uptake peak at 264°C and does not affect the peak at 320°C (curve *3*). A broad peak at a higher temperature of 460–470°C is also observed, which is characteristic of the reduction of bulk cobalt oxide. Further raising the CoO content to 7% leads to an increase in the peak intensities (curve *4*), particularly around 450°C. Note that variation of the amount of supported CoO changes only the hydrogen uptake peak intensities, while the peak positions remain unchanged (Fig. 7), as distinct from what we observed for the CuO/CeO_2 system [18].

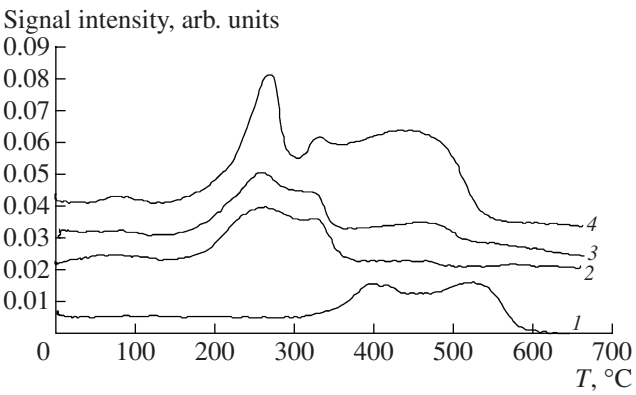

Fig. 7. TPR spectra of (*1*) CeO_2, (*2*) 1% CoO/CeO_2, (*3*) 2.5% CoO/CeO_2, and (*4*) 7% CoO/CeO_2.

The peaks at 264 and 320°C are likely due to the reduction of the small cobalt oxide particles (clusters) that resulted from the strong interaction between CoO and the support and to the reduction of CeO_2, respectively. The interaction between CoO and CeO_2 decreases the reduction temperatures of the CoO clusters and the CeO_2 support. The decrease in the CeO_2 reduction temperature is evident from the absence of hydrogen uptake peaks at 400 and 520°C in the case of the 1% CoO/CeO_2 sample (Fig. 7, curve *2*; compare with curve *1*) and from the fact that the hydrogen uptake between 200 and 300°C (table) is well above the calculated uptake necessary for the reduction of CoO or Co_3O_4 in the 1% CoO/CeO_2 sample. The observed synergetic effect (marked decrease in the reduction temperatures of both CoO and CeO_2) is also known for the CuO/CeO_2 system [18, 37, 38].

Thus, it is only in the system with the lowest CoO content (1%) that most of the CoO is bound to CeO_2, forming Co–Ce–O surface clusters. At higher CoO contents, an individual cobalt oxide phase, most likely Co_3O_4, forms on the surface.

The introduction of copper oxide into the CoO/CeO_2 catalyst markedly modifies the reduction process (Fig. 8). For example, the TPR spectrum of the 1% CuO/1% CoO/CeO_2 sample (curve *1*) shows no peaks due to the reduction of Co–Ce–O clusters (263°C) and CeO_2 (330°C) (see Fig. 7) and exhibits a narrow and strong peak with two maxima at 140 and 157°C, whose position falls into the region of copper oxide reduction in CuO/CeO_2 catalysts [18]. This peak is somewhat shifted to lower temperatures relative to the same peak for the 1% CuO/CeO_2 sample, and the positions of its maxima are the same as in the case of the 2.1% CuO/CeO_2 sample. A decrease in the reduction temperature of supported copper oxide that is due not to the increased CuO content, but to the effect of another metal oxide, was also observed for the $CuO/Fe_2O_3/CeO_2$ system [18].

TPR data for the CoO/CeO_2 and $CuO/CoO/CeO_2$ systems

Sample	T_{max}, °C	$[H_2] \times 10^4$, mol/g	$\Sigma[H_2] \times 10^4$, mol/g	$[H_2]$ (excess)* $\times 10^4$, mol/g
CeO_2	400	2.6	5.6	–
	526	3.0		
1% CoO/CeO_2	263, 330	5.2	5.5	4.1
	443	0.3		
2.5% CoO/CeO_2	264, 320	5.5	8.0	4.1
	466	2.5		
7% CoO/CeO_2	273, 337	~8.5	17.1	5.7
	450	~8.6		
Co_3O_4	352, 384	150	150	–
1% CuO/CeO_2	160, 194	6.7	6.7	5.5
1% CuO/1% CoO/CeO_2	140, 157	6.1	6.1	3.4
2.5% CuO/1% CoO/CeO_2	137, 147	7.9	7.9	3.5
1% CuO/2.5% CoO/CeO_2	165, 180	6.5	9.5	4.1
	234	1.6		
	434	1.4		
1% CuO/7% CoO/CeO_2	186	10.0	21.4	4.2
	269	7.4		
	443	4.0		
2.5% CuO/2.5% CoO/CeO_2	133, 155, 208	10.0	11.4	–
	440	1.4		
2.5% CoO/2.5% CuO/CeO_2	136, 160, 203	11.5	14.6	–
	350, 415	3.1		

* Excess over the amount of H_2 necessary for the reduction of the copper and/or cobalt cations.

Raising the CuO content to 2.5% shifts the hydrogen uptake peak to lower temperatures (T_{max} = 137 and 147°C) and increases the amount of hydrogen consumed (table). A comparison between the TPR data for the 1% CoO/CeO_2 sample (Fig. 7, curve *2*) and the 1% CuO/1% CoO/CeO_2 sample (Fig. 8, curve *1*) demonstrates that the amount of consumed hydrogen derived from the area of the narrow low-temperature peak is larger in the latter case (table) and is sufficient for the reduction of all of the supported oxides and the CeO_2 surface. This fact, in combination with the absence of peaks due to CoO/CeO_2 and CeO_2 reduction (263 and 330°C), suggests that there are strong interactions between copper and cobalt oxides and between these oxides and CeO_2 in the $CuO/CoO/CeO_2$ catalysts and that these interactions likely yield Cu–Co–Ce–O clusters.

As the CoO content of the 1% CuO/(1–7)% CoO/CeO_2 catalysts is increased, the main two-maximum peak in the TPR spectrum shifts to higher temperatures of ~165 and 180°C (Fig. 8, curves *2*, *3*). Peaks due to the reduction of Co-Ce–O clusters (234–269°C) and the Co_3O_4 phase (420–443°C) appear in the spectrum, which are typical of the CoO/CeO_2 system. For example, three peaks at 186, 269, and 443°C can be seen clearly in the spectrum of the 1% CuO/7% CoO/CeO_2 catalyst. These data suggest that, when the amount of cobalt oxide in the system exceeds the amount necessary for the formation of Cu–Co–Ce–O clusters, part of the CoO reacts with the CeO_2 surface without involving CuO, as in the case of the CoO/CeO_2 catalysts.

Comparing the results presented in Figs. 7 and 8, note that the addition of CuO to 7% CoO/CeO_2 diminishes both the Co–Ce–O cluster reduction peak at 269°C and the high-temperature peak at 443°C. According to earlier data [33], this can be due to the formation of the bulk mixed-spinel phase $Co^{2+}_{1-x}Cu^{2+}_x[Co^{3+}]_2O_4$, the reduction temperature of which is much lower than that of Co_3O_4 and falls into the range of the reduction temperatures of Cu-containing structures.

In order to find out, by the TPR method, how the properties of the catalyst depend on the order in which copper and cobalt oxides were supported on the CeO_2 surface, we examined 2.5% CuO/2.5% CoO/CeO_2 (sample 1) and 2.5% CoO/2.5% CuO/CeO_2 (sample 2). In the low-temperature region (100–250°C), the TPR spectra of these samples are almost identical. However, above 300°C, the spectrum of sample 2 has two weak peaks at 350 and 415°C, which are likely due to the reduction of the excess cobalt oxide that is not involved in the formation of surface Cu–Co–Ce–O clusters. It is possible that the supporting of cobalt oxide on the copper oxide–containing CeO_2 surface takes place less uniformly than the same process on pure CeO_2.

DISCUSSION

The catalytic activity of the CuO/CoO/CeO_2 and CoO/CeO_2 systems and the temperature of CO oxidation with oxygen in excess hydrogen depend on the nature and concentration of the cations supported on CeO_2. The data presented in Figs. 1 and 2 and in our earlier publication [17] suggest that the maximum catalytic activity decreases in the order CuO/CoO/CeO_2 ~ (5–6)% CuO/CeO_2 (98–99.5%) > CoO/CeO_2 (67–84%) > CeO_2 (35%). The decreases in catalytic activity in this order are accompanied by an increase in both the reaction temperature and T_{max} (140–160, 230–240, and 340°C, respectively). At the same time, TPD data for CO oxidation with surface oxygen [17] suggest the following order of CO_2 desorption onset temperatures (T_{CO_2}) for the CuO/CoO/CeO_2, CoO/CeO_2, and CeO_2 catalysts examined: 50, 200, 350°C. It is clear from a comparison of the T_{max} and T_{CO_2} sequences that the lower the CO_2 desorption onset temperature, the lower the CO oxidation temperature. This correlation suggests that CO oxidation in hydrogen-containing mixtures involves surface oxygen and that the carbonyl complexes Cu^+–CO and $Co^{\delta+}$–CO occurring on the catalysts may be intermediates of the reaction, in accordance with earlier reports [39, 40]. It is likely that adsorbed CO molecules form carbonyl complexes with the cations of Co–ox or Cu–Co–ox sites and are oxidized by oxygen of these sites to CO_2, which is desorbed into the gas phase, with the desorption activation energy depending on the metal–oxygen bond energy in these sites [41]. The TPD data allow the activation energies of CO and CO_2 desorption to be estimated from the equation $E_{des} = 25RT_{max,des}$ [42] (where R is the universal gas constant and $T_{max,des}$ is the desorption peak temperature). The activation energy of CO desorption upon the decomposition of the carbonyl complexes at $T_{max,des}$ = 373 K is 77 kJ/mol. The activation energy of CO_2 desorption is 87 kJ/mol for the CuO/CoO/CeO_2 catalysts at $T_{max,des}$ = 423 K, 105 kJ/mol for the CoO/CeO_2 catalysts at $T_{max,des}$ = 513 K, and 138 kJ/mol for CeO_2 at $T_{max,des}$ = 673 K. Therefore, CeO_2 surface oxygen has the highest bond energy and Cu–Co–ox oxygen has the lowest bond energy.

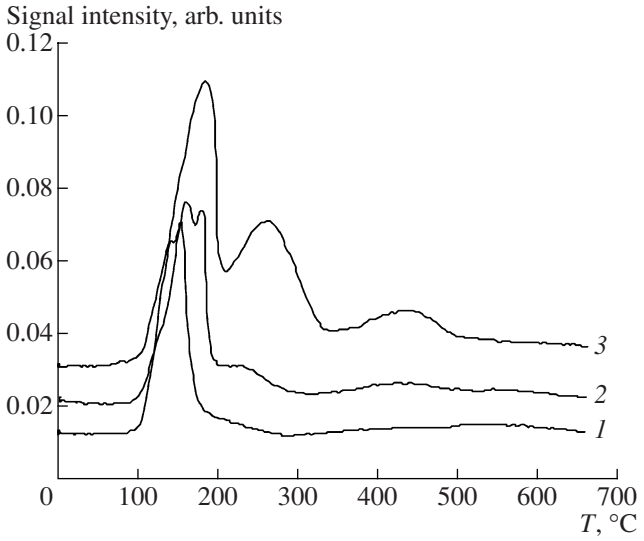

Fig. 8. TPR spectra of (*1*) 1% CuO/1% CoO/CeO_2, (*2*) 1% CuO/2.5% CoO/CeO_2, and (*3*) 1% CuO/7% CoO/CeO_2.

Let us consider, in greater detail, the nature of the CO oxidation sites in the catalysts. As follows from the above TPR data, the supporting of copper and cobalt oxides on the surface of CeO_2 crystallites no larger than 15 nm (according to x-ray diffraction data) yields Co–Ce–O or Cu–Co–Ce–O clusters. The reduction of the Cu–Co–Ce–O clusters with hydrogen (Fig. 8) takes place around 140°C. According to TPD data, the Cu–Co–ox sites observed on the surface of the CuO/CoO/CeO_2 catalysts are deactivated in hydrogen at the same temperature (Fig. 5). This coincidence is evidence that these sites are identical; that is, the low-temperature oxidation sites Cu–Co–ox are components of the Cu–Co–Ce–O clusters.

The same is true for the CoO/CeO_2 system. According to TPR and XPS data [11], at low CoO contents (1–2.5%), cobalt oxide forms surface Co–Ce–O clusters, whose properties are identical to the properties of the Co–ox sites discovered by CO TPD. These clusters are CO oxidation sites. They are more readily reducible with hydrogen (240°C) than the particles of the supported Co_3O_4 phase (400–500°C), which are present in the catalysts with high CoO contents (7%). According to TPD data, the amount of oxidized CO is in agreement with the cobalt cation content of the clusters, not with the cobalt cation content of the Co_3O_4 particles. As the CoO content of CeO_2 is raised from 1 to 2.5%, the Co^{2+} cation content of the clusters increases and the amount of oxidized CO increases simultaneously by a factor of 2.

The TPR and TPD data allow the number of cations in a cluster to be estimated for some catalysts. Under the assumption that the clusters of one kind have the

same elemental and quantitative compositions and that a single CO molecule can be oxidized on such a cluster, as was accepted in [43], the number of cations in one cluster will be equal to the ratio of the total number of cations in the clusters to the number of desorbed CO molecules. For the 2.5% CoO/CeO_2 sample, the number of cations in the clusters was estimated as the difference between the number of supported cations and the number of cations in the Co_3O_4 phase using data presented in the table. According to our calculations, a Co–Ce–O cluster can contain ~3 Co^{2+} cations. The 1% CuO/2.5% CoO/CeO_2 sample has two types of clusters, namely, Co–Ce–O and Cu–Co–Ce–O. The first type contains three Co^{2+} cations, and the second can contain two or three Cu^{2+} cations. We were unable to determine the number of Co^{2+} cations in one cluster of the second type because the total number of cobalt cations in these clusters was unknown.

It is likely that Co adsorbed on a cluster is oxidized by oxygen of this cluster, even though the literature dealing with CO oxidation on CeO_2-containing catalytic systems suggests models taking into account oxygen migration on the surface and oxygen diffusion from the bulk to the support surface [44]. The participation of bulk oxygen in the reaction is unlikely because of the smallness of the diffusion coefficient at 50–200°C. TPD data demonstrate that the amount of CO oxidized with the surface oxygen of the 1% CuO/2.5% CoO/CeO_2 catalyst (7.2×10^{17} m^{-2}) does not exceed the amounts of the supported oxides CuO and CoO (4×10^{18} m^{-2}).

The oxidation of CO on CuO/CeO_2 catalysts may involve the bridging oxygen of Cu^{2+}–O^{2-}–Cu^{2+} clusters [39, 40], Cu^{2+}–O^{2-}–Ce^{4+} clusters [45], or $V^{\bullet\bullet}$–O^{2-}–Cu^{2+} (where $V^{\bullet\bullet}$ is an anionic vacancy on the CeO_2 surface) [46]. The first scheme was considered for CuO/CeO_2 catalysts [17]. The totality of data obtained for the CuO/CeO_2, $CuO/CoO/CeO_2$, and $CuO/Fe_2O_3/CeO_2$ systems led to some assumption as to the formation of active sites in these catalysts. The highest CO conversion (98–99%) is observed at 140–160°C on the catalysts 5%CuO/CeO_2 [17], 2.5% CuO/2.5% Fe_2O_3/CeO_2 [18], and 2.5% CuO/2.5% CoO/CeO_2. Therefore, part of the copper oxide in 5% CuO/CeO_2, the most active sample, can be replaced with iron or cobalt oxide without reducing the activity of the catalyst in spite of the fact that the CO conversion on the 2.5% Fe_2O_3/CeO_2 catalyst is low and is comparable with the CO conversion over CeO_2 and CO oxidation on the 2.5% CoO/CeO_2 catalyst requires a much higher temperature (240°C). The fact that the highest conversion of CO into CO_2 on the catalysts 5% CuO/CeO_2, 2.5% CuO/2.5% Fe_2O_3/CeO_2, and 2.5% CuO/2.5% CoO/CeO_2 is achieved at the same temperature suggests that the bond energies of oxygen in clusters with different cationic compositions are similar. Apparently, the oxidation reaction in all systems takes place on one type of fragment, probably the Cu^{2+}–O^{2-}–Ce^{4+} site, which is present not only in the CuO/CeO_2 catalysts, but also in the Cu–Co–Ce–O and Cu–Fe–Ce–O clusters. If this is the case, the effect of the introduction of iron or cobalt oxide into CuO/CeO_2 can be due to the replacement of part of the copper cations in the Cu–Ce–O clusters with Fe or Co cations, resulting in the formation of Cu–Co–Ce–O or Cu–Fe–Ce–O clusters, in which oxygen transfer to the Cu^{2+}–O^{2-}–Ce^{4+} active sites takes place more readily. This is suggested by TPR data for the 2.5% CuO/2.5% CoO/CeO_2 and 2.5% CuO/2.5% Fe_2O_3/CeO_2 catalysts [18], including the decrease in the copper oxide reduction temperature, the hydrogen uptake exceeding the uptake necessary for the reduction of the supported oxides, and the absence of the high-temperature peak due to CeO_2 reduction, as well as by the reoxidation of reduced copper at room temperature. The fact that the temperature range of the reaction in the maximum-conversion region is wider for these catalysts than for CuO/CeO_2 is due to the properties of oxygen in the resulting clusters and is a very significant factor in stable catalyst operation at T_{max} in an exothermic reaction. The mechanism of this effect needs further investigation.

According to TPD data, the number of active sites, though determined by the amount of supported CuO, is larger in the 2.5% CuO/2.5% CoO/CeO_2 and 2.5% CuO/2.5% Fe_2O_3/CeO_2 catalysts than in the 2.5% CuO/CeO_2 catalyst and is equal to the number of active sites in 5% CuO/CeO_2. This may be explained by the decrease in the cluster size due to the specific interaction between supported CuO and the CoO/CeO_2 or Fe_2O_3/CeO_2 surface or by the decrease in the Cu/Ce ratio in the clusters due to the replacement of part of the copper cations by cobalt or iron cations.

A comparison between the catalytic activity data for the CoO/CeO_2 samples in CO hydrogenation and the TPR data (Figs. 1, 7) indicates that the onset temperature of the reaction on CoO/CeO_2 (>270°C) is in the CoO reduction temperature range (270–450°C). This is in agreement with the universally accepted Fischer–Tropsch mechanism, according to which the dissociative adsorption of CO, necessary for CH_4 formation, takes place on cobalt metal clusters. The introduction of copper oxide into the CoO/CeO_2 catalysts with a low CoO content (1–2.5%) causes cobalt binding into Cu–Co–Ce–O clusters, and CO hydrogenation is thus hampered because of the absence of monometallic cobalt particles. At higher CoO contents (3.5–7%), the catalysts contain extra Co-containing active sites, and it is these sites where CO hydrogenation takes place at high temperatures. The effect of copper oxide in these systems is not restricted to CO oxidation into CO_2. Copper oxide shifts the CO hydrogenation range by 80–100°C to lower temperatures. It is possible that, in the supporting of CuO, the formation of Cu–Co–Ce–O clusters is accompanied by the dispersion of the cobalt oxide particles forming CO hydrogenation sites. This makes them more readily reducible and, accordingly, lowers the reaction temperature.

ACKNOWLEDGMENTS

The authors are grateful to Z.T. Fattakhov for specific surface area measurements and to D.P. Shashkin for x-ray diffraction analyses.

This study was supported by the Russian Foundation for Basic Research (grant no. 07-03-01074).

REFERENCES

1. Kahlich, M.J., Gasteiger, H.A., and Behm, R.J., *J. Catal.*, 1997, vol. 171, p. 93.
2. Lee, S.J., Mukerjee, S., Ticinelli, E.A., and VcBreen, J., *Electrochim. Acta*, 1999, vol. 44, p. 3283.
3. Avgoropoulos, G., Ioannides, T., Matralis, H., Baatista, J., and Hocevar, S., *Catal. Lett.*, 2001, vol. 73, p. 33.
4. Igarashi, H., Uchida, H., Suzuki, M., and Watanabe, M., *Appl. Catal., A*, 1997, vol. 159, p. 159.
5. Ito, S.-I., Fujimori, T., Nagashima, K., Yuzaki, K., and Kumimori, K., *Catal. Today*, 2000, vol. 57, p. 247.
6. Cheng, W.H., *React. Kinet. Catal. Lett.*, 1996, vol. 58, p. 329.
7. Torres, R.M., Sachez, A., Ueda, K., Tanaka, K., and Haruta, M., *J. Catal.*, 1997, vol. 168, p. 125.
8. Liotta, L.F., di Cario, G., Pantaleo, G., and Deganello, G., *Catal. Commun.*, 2005, vol. 6, p. 329.
9. Kang, M., Song, M.W., and Lee, C.H., *Appl. Catal., A*, 2003, vol. 251, no. 1, p. 143.
10. Tang, C.-W., Kuo, C.-C., Kuo, M.-C., Wang, C.-B., and Chien, S.-H., *Appl. Catal., A*, 2006, vol. 309, p. 37.
11. Natile, M.M. and Glisenti, A., *Chem. Mater.*, 2005, vol. 17, no. 14, p. 3403.
12. Liu, W. and Flytzani-Stefanopoulos, M., *J. Catal.*, 1995, vol. 153, p. 304.
13. Liu, W. and Flytzani-Stefanopoulos, M., *J. Catal.*, 1995, vol. 153, p. 317.
14. Sedmak, G., Hacevak, S., and Levec, J., *J. Catal.*, 2003, vol. 213, p. 135.
15. Ratnasamy, P., Srinavas, D., Satyanarayana, C.V.V., Manikandak, P., Kumaran, R.S.S., Sachin, M., and Shetti, V.N., *J. Catal.*, 2003, vol. 204, p. 455.
16. Marban, J. and Fuertes, A.B., *Appl. Catal., B*, 2005, vol. 57, no. 1, p. 34.
17. Il'ichev, A.N., Firsova, A.A., and Korchak, V.N., *Kinet. Katal.*, 2006, vol. 47, no. 4, p. 602 [*Kinet. Catal.* (Engl. Transl.), vol. 47, no. 4, p. 585].
18. Firsova, A.A., Il'ichev, A.N., Khomenko, T.I., Gorobinskii, L.V., Maksimov, Yu.V., Suzdalev, I.P., and Korchak, V.N., *Kinet. Katal.*, 2007, vol. 48, no. 2, p. 298 [*Kinet. Catal.* (Engl. Transl.), vol. 48, no. 2, p. 282].
19. Jansson, J., Palmavist, A.E.C., Fridell, E., Skoglundh, M., Osterlund, L., Thormahlen, P., and Langer, V., *J. Catal.*, 2002, vol. 211, no. 2, p. 387.
20. Aneggi, E., Llorca, J., Boaro, M., and Trovarelli, A., *J. Catal.*, 2005, vol. 234, p. 88.
21. Tret'yakov, I.I., Shub, B.R., and Sklyarov, A.V., *Zh. Fiz. Khim.*, 1970, vol. 44, p. 2112.
22. *Handbuch der preparativen anorganischen Chemie*, von Brauer, G., Ed., Stuttgart: Ferdinand Enke, 1981.
23. Li, C., Sakata, Y., Domon, T.K., Maruya, K., and Onishi, T, *J. Chem. Soc., Faraday Trans. 1*, 1989, vol. 85, no. 4, p. 929.
24. Mouaddib, N., Perrichon, V., and Primmet, M., *J. Chem. Soc., Faraday Trans. 1*, 1989, vol. 85, no. 10, p. 3413.
25. Carrington, A. and McLachlan, A.D., *Introduction to Magnetic Resonance*, New York: Harper & Row, 1967.
26. Martinez-Arias, A., Soria, J., Seoane, X.L., Arcoya, A., and Cataluna, R., *J. Chem. Soc., Faraday Trans. 1*, 1995, vol. 91, no. 11, p. 1679.
27. Il'ichev, A.N., Shibanova, M.D., Ukharskii, A.A., Kulizade, A.M., and Korchak, V.N., *Kinet. Katal.*, 2005, vol. 46, no. 3, p. 414 [*Kinet. Catal.* (Engl. Transl.), vol. 46, no. 3, p. 387].
28. Martinez-Arias, A., Fernandez-Garcia, M., Soria, J., and Conesa, J., *J. Catal.*, 1999, vol. 182, p. 367.
29. Kucherov, A.V. and Slinkin, A.A., *Usp. Khim.*, 1992, vol. 61, no. 9, p. 1687.
30. Shyu, J.Z., Weber, W.H., and Gandhi, H.S., *J. Phys. Chem.*, 1988, vol. 92, no. 7, p. 4964.
31. Laachir, A., Perrichon, V., Badri, A., Lamotte, J., Catherine, E., Lavalley, C., Fallah, J., Hilaire, L., le Normand, F., Guemere, E., Sauvion, G.N., and Touret, O., *J. Chem. Soc., Faraday Trans.*, 1991, vol. 87, no. 10, p. 1601.
32. Perrichon, V., Laachir, A., Bergeret, G., Frety, R., Tournayan, L., and Touret, O., *J. Chem. Soc., Faraday Trans.*, 1994, vol. 90, no. 5, p. 773.
33. Fierro, G., LoJacono, M., Inversi, M., Dragon, R., and Porta, P., *Top. Catal.*, 2000, vol. 10, p. 39.
34. Riva, R., Miessner, H., Vitali, R., and Aero, G., *Appl. Catal., A*, 2000, vol. 196, p. 111.
35. Arnoldy, P. and Maulijn, J.A., *J. Catal.*, 1985, vol. 93, p. 38.
36. Thormahlen, P., Skoglundh, M., Fridell, E., and Anderson, B., *J. Catal.*, 1999, vol. 188, p. 300.
37. Luo, M-F., Zhong, Y-J., Yuan, X-X., and Zheng, X-M., *Appl. Catal., A*, 1997, vol. 162, p. 121.
38. Zimmer, P., Tschope, A., and Birringer, R., *J. Catal.*, 2002, vol. 205, p. 339.
39. Bobrov, N.N., Davydov, A.A., Ione, K.G., et al., *Izv. Akad. Nauk SSSR, Ser. Khim.*, 1975, no. 4, p. 748.
40. Davydov, A.A., Budneva, A.A., and Sokolovskii, V.D., *Kinet. Katal.*, 1989, vol. 30, no. 6, p. 1407.
41. Krylov, O.V., *Geterogennyi kataliz* (Heterogeneous Catalysis), Moscow: Akademkniga, 2004.
42. Kislyuk, M.U. and Rozanov, V.V., *Kinet. Katal.*, 1995, vol. 36, no. 1, p. 89.
43. Dow, W.-P., Wang, Y.-P., and Huang, T-J., *J. Catal.*, 1996, vol. 160, p. 155.
44. Giordano, F., Trovarelli, A., de Leitenburg, C., and Giona, M., *J. Catal.*, 2000, vol. 193, p. 273.
45. Martinez-Arias, A., Fernandez-Garcia, M., Galvez, O., Coronado, J.M., Anderson, J.A., Conesa, J.C., Soria, J., and Munuera, G., *J. Catal.*, 2000, vol. 195, p. 207.
46. Dow, W.-P. and Huang T.-J., *J. Catal.*, 1996, vol. 160, p. 171.